Single Phase Formation of CuInS$_2$ Nanoparticles: Structural, Morphological, Thermal Studies with Annealing Effect

P. Suchismita Behera[1], Desapogu Rajesh[2], S. Karthikeyan[3], C. S. Sunandana[2*] and D. Bharathi Mohan[1*]

[1]*Department of Physics, School of Physical, Chemical and Applied Sciences, Pondicherry University, R. V. Nagar, Kalapet, Puducherry-605 014, India*
[2]*School of Physics, University of Hyderabad, Hyderabad, A.P-500 046, India*
[3]*Department of Electrical and Computer Engineering, University of Minnesota, 5-151 Keller Hall, 200 Union Street SE, Minneapolis, MN 55455-0170.*

Abstract : *Single phase of CuInS$_2$ nanoparticles was prepared by solid state melt growth process. The structural, morphological and elemental analyses were studied by using X-ray diffraction, Field Emission Scanning Electron Microscope and Energy Dispersive Analysis of X-rays. The differential thermal analysis (DTA) and thermo gravimetric analysis (TGA) confirms the phase transformation and stability of CuInS$_2$ with its annealing effect at 200°C. Micro-Raman studies evidencing a strong Raman A$_1$ mode at 285 cm^{-1} and 302 cm^{-1}, corresponds to totally symmetric vibration of anion − sub lattice of CuInS$_2$ structure.*
Keywords: Chalcopyrite type CuInS2 nanoparticles, Crystal Structure, Surface morphology, Elemental Composition, Microstructure and phase Transition

I. INTRODUCTION

Semiconductor nanoparticles are potential applications in science and technology due to their size and shape dependent properties [1, 2]. Because of their tunable absorption in the visible and IR range of the solar spectrum, semiconductor nanocrystals are considered to be an interesting absorber material for solar cell [3-5]. However, to the best of our knowledge most of the materials like cadmium and lead chalogenides have a drawback of containing highly toxic components that severely restricts their possible applications [6]. A possible alternative material, being less toxic, but having a tunable absorption in the visible range, is copper indium disulfide (CIS). Solar cell technologies using an I–III–VI chalcopyrite semiconductor have made rapid progress in recent years. In particular, CuInS$_2$ (CIS) based solar cells have been extensively reported in comparison to other chalcopyrite semiconductor based solar cells. Compared to other selenium chalcopyrite such as CuInSe$_2$, CuInS$_2$ is even more favorable for photovoltaic solar power. Substituting the problematic selenium by non-toxic sulphur, CuInS$_2$ is more environment-friendly than CuInSe$_2$ [7,8]. The open circuit voltage of CuInS$_2$ solar cells is theoretically higher than that of CuInSe$_2$ and Cu(In, Ga)Se$_2$ based solar cells and can efficiently absorb the solar energy. Due to a superior band gap of about 1.5 eV, matching almost ideally to the solar spectrum, CuInS$_2$ has in principle the highest conversion efficiency among the Cu chalcopyrite-based solar cells. Theoretically it has been predicted that the energy conversion efficiency of a CuInS$_2$ solar cell can be as high as 26%. Any type of device fabrication, it is essential that the material is grown defect free, either in the form of single phase of powder or thin films, as well as characterized using different techniques before it is put to any technical use. It is well known that the device properties of CuInS$_2$-based solar cells are highly affected by their stoichiometric Composition. In contrast to the physical and chemical vapour deposition techniques, solid state reaction method is a simplest, inexpensive technique. In the present work we reported structural, morphological, thermal properties of CuInS2 nanoparticles synthesized by a convenient solid state melt growth process.

II. EXPERIMENTAL

2.1 Material and Methods:

Synthesis of CuInS$_2$ Nanoparticles

Ingot of CuInS$_2$ was prepared in a high temperature furnace after mixing high pure (99.99 %) elements such as Cu, In and S in 1:1:2 stoichiometry ratio in a vacuum sealed quartz ampoule at the pressure of 1E-3 mbar. To avoid explosion due to sulphur vapour pressure, a step heating and cooling process was followed.

Heating Steps:
28 ^{o}C - 50 ^{o}C : 5.0 ^{o}C / minute,   50 ^{o}C - 350 ^{o}C : 0.5 ^{o}C /minute,
350 ^{o}C - 1150 ^{o}C : 10.0 ^{o}C / minute (kept at 1150 ^{o}C for 2 hrs)

Cooling Steps:
1150 ^{o}C- 28 ^{o}C : 10 ^{o}C / minute

Slow heating process was crucial between 100 °C to 300 °C because of the exothermic reaction between sulphur and indium. The melt was kept at 1150 °C for 2 h in order to achieve a complete homogeneous mixture. Ingot was formed after the sample was cooled slowly. Later on, CIS ingot was crushed using agate mortar and pestle and thus a homogeneous composition of $CuInS_2$ phase was obtained. As prepared composition was then heat treated at temperatures 200°C under vacuum (1E-2 mbar). Sample codes of as prepared and annealed compositions are given in Table 1.

2.2 Characterization Techniques:

X-Ray Diffraction (XRD) patterns of as prepared $CuInS_2$ (CIS) powder samples were recorded by Philips PW 1830 XRD instrument using monochromatic Cu-K$_\alpha$ (λ-1.541 Å) radiation at a scanning rate of 2° per minute in 2θ ranging from 10° to 80°. The surface morphology was examined by Field Emission Scanning Electron Microscopy (FE-SEM) and the elemental composition was quantified by Energy Dispersive X-ray analysis (EDX) using ZEISS-ULTRA 55. Micro Raman scattering measurements performed at room temperature with a Jobin−Yvon Horiba spectrometer coupled with an Olympus metallographic microscope, using the green line of an Ar$^+$ laser (λ = 514 nm) as excitation light. The objective used (×100, NA 0.95), yields a nearly sub-micron spot size on the sample spectra were obtained in the backscattering configuration, collecting light from all possible polarisations. Under these conditions, the depth investigated by the Raman microprobe is determined by optical absorption of light in $CuInS_2$, which is about 1/100 nm. Excitation power of light on the sample was about 1.0 mW, for which no thermal effects in the spectra were observed. Finally, the spectra was compared with those measured at the same conditions on single crystal stoichiometric $CuInS_2$. The infrared (IR) spectrum of CIS samples was recorded in the wave number range from 4000 cm^{-1} to 400 cm^{-1} using Perkin Elmer Spectrum GX Fourier transform infrared (FTIR) spectrometer. DSC and TG thermograms of $CuInS_2$ powder samples were observed by NETZSCH-STA 449 F3 ranging from temperature 100°C to 1500°C.

III. RESULTS AND DISCUSSION

3.1 Crystal Structure, Surface Morphology and Elemental Composition:

The XRD spectra in figure 1 shows that sample B-CIS3 confirms the formation of single phase CIS crystal structure whereas sample B-CIS1 shows CIS as well with other phases such as In_2O_3, CuO, CIS, In_2S_3. The reason is following that B-CIS3 prepared under vacuum sealing prevented oxidation during the formation process whereas it was not in case of B-CIS1. Therefore, it is must to carry out the synthesis process under vacuum for obtaining a single phase of $CuInS_2$. According to figure 1, a predominant peak (2θ =27.93°) is assigned to (*112*) reflection of $CuInS_2$ phase. Chalcopyrite structure was confirmed through characteristic peaks which are due to (*101*), (*103*), (*211*), (*213*) crystal planes corresponding 2θ equals to (*17.98*), (*28.95*), (*37.38*), (*44.08*) respectively [9, 10]. The growth of chalcopyrite structure of $CuInS_2$ was confirmed after comparing the crystal planes positions with Joint Committee for Powder Diffraction Data (JCPDS), Card Number: 89-6095. Chalcopyrite structure is a distorted double zinc blende lattice with the lattice parameter $c > 2a$, which is in good agreement with our calculated results. Tetragonal distortion (η) of the lattice is calculated from the equation known as 2-(c/a). The unit cell lattice parameters (a, c, η and density) were calculated from XRD and compared in Table 2. The unit lattice parameters observed be in agreement well with the standard data (a = 5.523 Å and c = 11.14 Å, volume = 339.57×10^{-30}m^3 and density = 4.748×10^{-24} gm. / cm^3). It is very clear that the average particle size increases for the sample annealed at 200°C, but corresponding density is reduced. Also there is a small increase in a and c values and decrease in the volume of unit cell of CIS structure observed in B-CIS6 sample. Tetragonal distortion (η) is found to be ≈1 confirming the arrangement of extended double lattice structure of $CuInS_2$. In Figure 2, sample B-CIS6 exhibits very sharp peaks with increased intensities as compared to sample B-CIS3. Because, the crystalinity is improved in B-CIS6 with the effect thermal annealing at 200°C. Broad peaks observed in B-CIS3 sample are due to the presence of smaller size of particles, whereas sharp peaks with high intensity are due to the presence of bigger particles [11]. The average particle size of CIS was calculated from Scherrer formula showing in the range of 80 - 150 nm. Moreover, there is also a shift observed in 2θ position in all peaks with annealing. The morphological studies of $CuInS_2$ samples were performed by FE-SEM technique, which are shown in Fig.3. Sample B-CIS1 exhibits flower like morphology but not as individual particle could be due to mixed phase formation of In_2O_3, CuO, CIS, In_2S_3. In B-CIS3, it is very comprehensible that the particle size is very small in B-CIS3 than from B-CIS6 correlating the particle size determined from XRD pattern. It was clearly revealed that an increased particle size after post annealing at 200°C for 1 hr. Also we can see the uniformity in the particle size [12]. The compositional analysis by EDAX for the all samples is shown in Table 3. From Figure 4 It was observed that the stoichiometric ratio between copper, indium and sulphur could be accurately controlled from the starting composition of the precursor. According to table 3, annealed sample B-CIS6 shows the decrease of sulphur and indium concentration and

increase of copper concentration as compared to unannealed sample B-CIS3. Sulphur deficiency is noticed significantly in the post deposition annealed sample.

3.2 FTIR Study:

FTIR spectroscopy has been used to detect the presence of organic impurities and the chemical structure of CuInS$_2$ samples as shown in Fig. 5. The FTIR spectra of samples B-CIS1 and CIS4 reveal absence of lattice vibrations caused by CuInS$_2$ in the spectral range 4000–400 cm^{-1}. However, it shows vibrations at 1126 and 657 cm^{-1} could be coupled with sulphate (SO$_4$) group [13]. The FTIR transmission in annealed CIS sample decreases as compared to un-annealed CIS. Peaks at 3410 cm^{-1} and 3365 cm^{-1} show the presence of both copper and indium complexes. The spectrum also indicates the absorptions at 1126 cm^{-1} and 1129 cm^{-1} which is assigned to CuSO$_4$. The spectrum shows the absorption at 656 cm^{-1} and 657 cm^{-1} belongs to Cu$_2$O group. In sample B-CIS3 and B-CIS6, IR spectrum revealed the possible vibrations at 3400 cm^{-1} and 3226 cm^{-1} which belongs to the presence of both copper and indium. In the post deposition annealed CuInS$_2$ sample, the IR transmission peak was broad and left shifted. The vibration bands at 1100 cm^{-1} and 1126 cm^{-1} for In-complex and 1000 cm^{-1} and 870 cm^{-1} for Cu-complex due to C=S stretching vibrations [14]. It is also indicated that the absorptions at 1600 cm^{-1}, 1684 cm^{-1} are due to CuS group and 627 cm^{-1} is due to Cu$_2$O group [13].

3.3 Micro-Raman Measurements:

Figure 6 represents Raman spectra of as synthesized CIS compositions at different conditions. Sample B-CIS1 exhibits two broad peaks at 130 cm^{-1} and 302 cm^{-1} whereas single peak is obtained in sample B-CIS3 at 285 cm^{-1}. An intense mode at ~302 cm^{-1} in sample B-CIS1 has been previously noticed for indium rich CuInS$_2$ samples [15, 16–17] and β-In$_2$S$_3$ presents a strong peak close to 302 cm^{-1} with A$_1$ symmetry [18]. Raman peak is observed at 285 cm^{-1} corresponds to the symmetric A$_1$ mode (pure anion vibration) of the sulphur lattice and found to be dominating Raman mode in device-quality CuInS$_2$ material [19]. The post deposition annealed samples B-CIS4 and B-CIS6 shows high intensity peaks as compared to the without annealed CIS sample B-CIS1 and B-CIS3. Two additional peaks are observed in B-CIS6 sample at 300 cm^{-1} and 363 cm^{-1}. Also it can be seen that the mode which belongs to cation-anion vibrations E and B$_2$ mode is not observed at 343 cm^{-1}. Almost there is not so much change observed in annealed samples [19]. From table 4, different peaks of the Raman spectra of CuInS$_2$ were fitted to Gaussian curve and the full-widths at half maximum (FWHM) was estimated from each peak. The FWHM of the peak at 285 cm^{-1} increases with annealing temperature. Intensity of the Raman modes are increasing with increasing annealing temperature as due to increased crystallinity.

3.4 Thermal Analysis:

Data derived from TG revealed the onset temperature, the temperature corresponding to the point maximum rate of weight loss (MRW). Two main thermal events are of importance in DSC plots, an endothermal event assignable to the melting point of a solid precursor and an exothermal event assignable to the decomposition of the precursor. Figure 7 shows the sample B-CIS1 which consist of some mixed oxide phases. The observed thermographs are corresponding to the characteristic properties of mixed phases of In$_2$O$_3$, CuO, CuS, CuInS$_2$ and In$_2$S$_3$ in accordance with XRD. The initial weight loss is 0.2%, afterwards it is constant, then again weight loss of 2% is obtained due to the desorption of the adsorbed gas. DSC curve exhibits two endothermic peaks and two exothermic peaks at 940°C, 1200°C, 1280°C and 1470°C respectively, could be due to the phase transformation, melting and oxidation of the above mentioned oxide phases. TG represents mass loss and gain by 2 % in range from 500°C to 900°C in post deposition annealed sample (B-CIS4). Here, a broad endothermic peak and a sharp endothermic peak are observed at 900°C and 1190°C respectively. The results are very similar as compared to B-CIS1, however exothermic peaks disappears at 1300°C and 1470°C in sample B-CIS1. B-CIS3 shows a broad endothermic peak in the range starting from 400°C to 1000°C and the dip is observed at 837.3°C. A sharp exothermic peak at 981.6°C is the phase transformation of ternary CIS compound. Above this temperature, the most thermodynamically stable phase is sphalerite, where Cu and In atoms are randomly distributed in tetragonal cation sublattice. The typical value of phase transition temperature is 927°C however here it is 54.6°C higher which could be due to the thermal stability of nanostructure could be possible in nanoscale. TG curve shows 1% of mass loss up to 800°C and then decreases by 4% recorded up to 1000°C. Decrease in the weight loss after 800°C could be due to the structural transformation which is observed up to 1000°C. B-CIS6 sample shows DSC curve which initially decreases up to 1000°C and then two endothermic peaks are observed at 1020°C and 1360°C. The presence of endothermic peaks are due to the melting points of the sphalerite stable phase. TG curve exhibit significant weight loss at temperatures 1020°C and 1360°C are matching with the endothermic peaks of DSC curve, confirming the melting points of the most stable sphalerite phase [20].

IV.   FIGURES AND TABLES

Table 1. Sample codes of as prepared and annealed CuInS$_2$ nanoparticles

S. No	Process	As prepared powder	Annealed at 200 °C
1	Without Vacuum sealing	B-CIS1	B-CIS4
2	With vacuum sealing	B-CIS3	B-CIS6

Table 2: List of unit lattice parameters such as *a*, *c*, volume, density, grain size and tetragonal distortion of CIS samples.

Sample	*a* (Å)	*c* (Å)	Volume (10^{-30} m^3)	Density (10^{-24} gm/cm^3)	Avg. Particle Size (nm) ± error	η
B-CIS3	5.523	11.042	336.885	4.780	28.0 ± 1.4	0.9984
B-CIS6	5.526	11.043	337.293	4.775	48.5 ± 1.0	0.9903

Table 3: Quantitative analysis of CIS powders from EDAX measurements.

Sample	Cu (in atomic%)	In (in atomic %)	S (in atomic %)
B-CIS 3	25.69	28.41	45.90
B-CIS 6	36.78	24.12	39.10

Table 4: Raman shift, Intensity and FWHM of corresponding CIS samples.

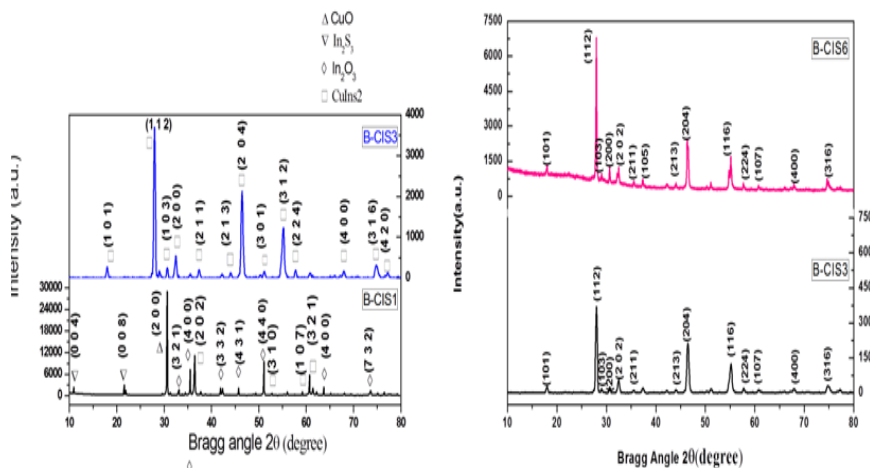| Sample	Raman Shift(cm^{-1})	Intensity	FWHM
B-CIS1	130	423	5.43
	302	208	19.48
B-CIS3	285	122	2.22
B-CIS4	128	514	5.75
	299	218	11.12
B-CIS6	283	144	6.09
	364	127	2.8

Figure 1: X-Ray Diffraction patterns of as prepared CuInS$_2$ samples. Samples B-CIS3 is matching with standard pattern of single phase of CuInS$_2$ crystal structure while B-CIS1 shows many oxide phases because this sample was not synthesized under vacuum condition.

Figure 2: XRD patterns of as prepared CuInS$_2$ samples before (B-CIS3) and after annealing (B-CIS6). From the diffraction intensity comparison between B-CIS3 and B-CIS6, it is clear that crystallization is improved after annealing B-CIS3 at 200^0 C for 1 hr.
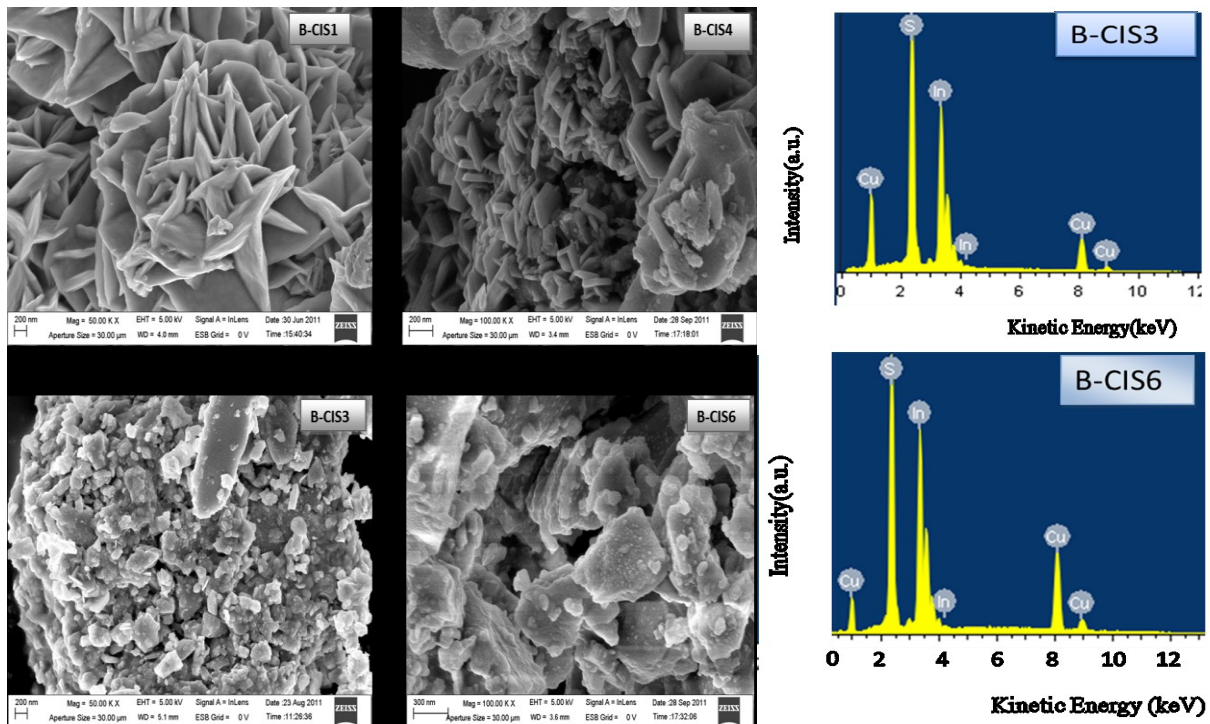
Figure 3: FESEM images of as prepared (B-CIS1, B-CIS3) and post annealed (B-CIS4, B-CIS6) CuInS₂ samples. Particle size is increases with annealing process as due to crystallization of CIS nanoparticles.

Figure 4: EDAX spectrum of prepared (B-CIS3) and post deposition annealed CuInS₂ nanoparticles (B-CIS6).
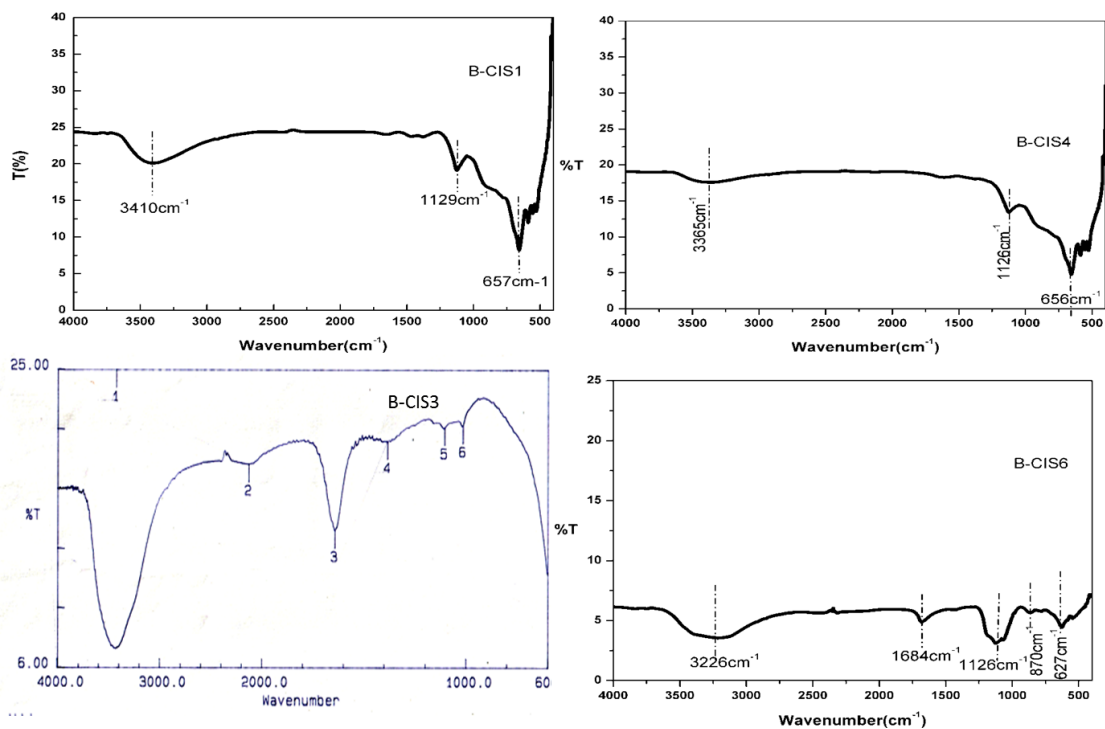
Figure 5: FTIR spectra for CuInS₂ samples: CIS without vacuum sealing (B-CIS1), CIS   without vacuum sealing annealed at 200°C (B-CIS4) and as prepared and post deposition annealed CuInS₂ samples (B-CIS3 and B-CIS6) by step heating process.
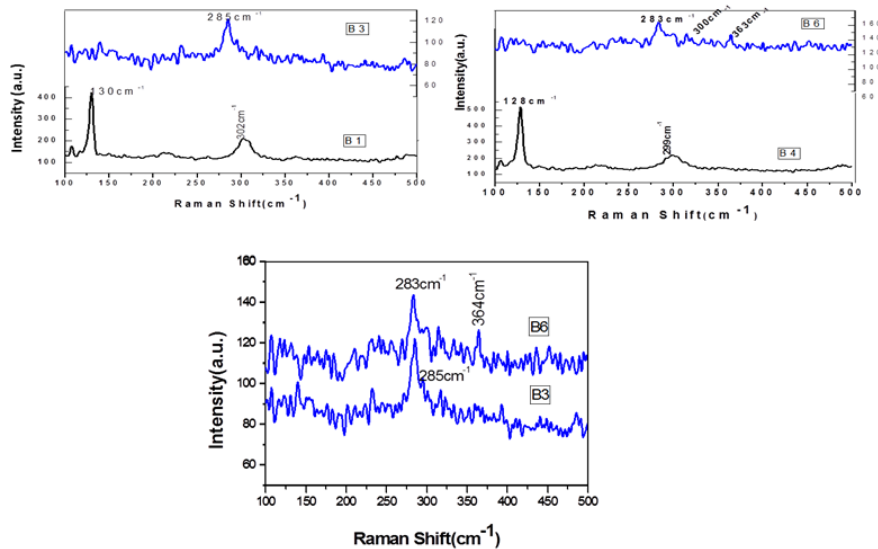
Figure 6: Raman spectra of as prepared CuInS₂ sample: B1 (B-CIS1) - CIS without vacuum sealing, B3 (B-CIS3) - Step heating under vacuum, B4 (B-CIS4) - CIS without vacuum sealing and annealed at 200°C and B6 (B-CIS6) - Step heating under vacuum and annealed at 200°C.
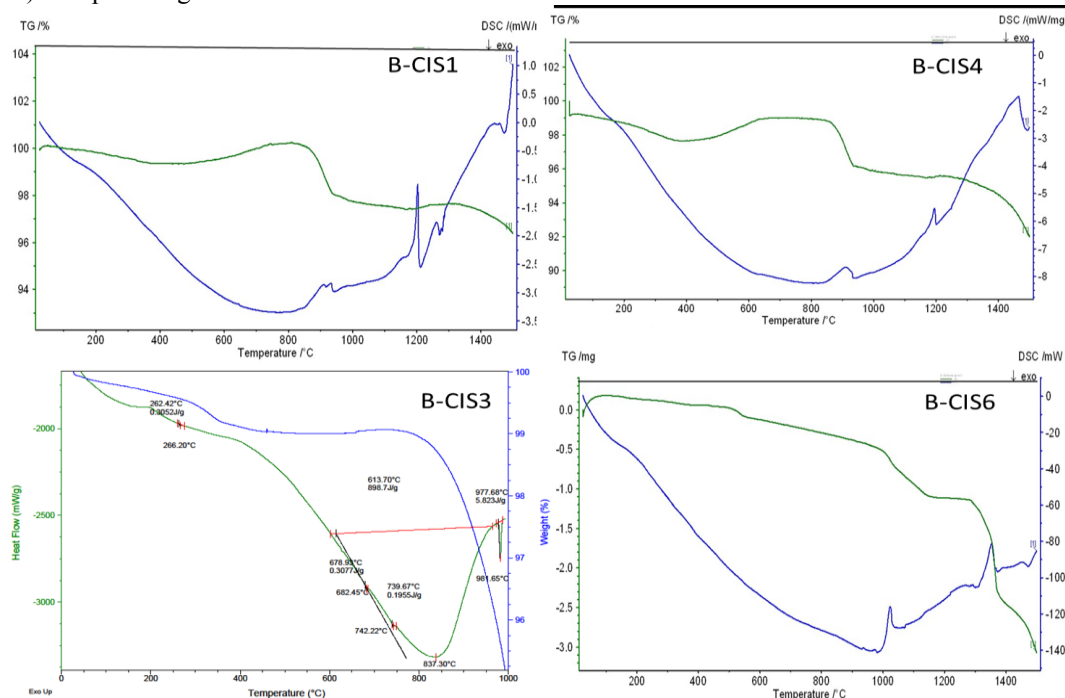
Figure 7: DSC–TG thermographs of as prepared and annealed at 200°C CuInS2 powder samples B-CIS1, B-CIS3 and B-CIS4, B-CIS6 respectively.

V.   CONCLUSION

The single phase of CuInS₂ ingot was prepared by step heating and cooling process under high vacuum sealing. It was compared to the composition prepared without vacuum sealing and post deposition annealing at 200°C. Chalcopyrite structure is conformed through characteristic peaks arises due to the presence of (101), (103), (211) planes. The average particle size is ranging from 80 to 150 nm. The surface morphology and elemental composition were investigated through FESEM and EDAX analysis respectively. Raman peaks at 285 cm^{-1} and 283 cm^{-1} corresponds to the symmetric A₁ mode (pure anion vibration) of the sulphur lattice and found to be dominating Raman mode in device-quality CuInS₂ material. TG curve exhibit significant weight loss at temperatures 1020°C and 1360°C are matching with the endothermic peaks of DSC curve, confirming the melting points of the most stable sphalerite phase, which is nothing but the change of phase transformation from chalcopyrite to sphalerite phase.

REFERENCES

[1] A. P. ALIVISATOS, J. PHYS. CHEM., **100** (1996) 13226.
[2] C. B. Murray, C. R. Kagan, M.G. Bawendi, Annu. ReV. Mater. Sci., **30** (2000) 545.
[3] W.U. Huynh, J.J. Dittmer, A.P. Alivisatos, Science, **295** (2002) 2425.
[4] Arici, E.Meissner, D.Schaffler, F.Sariciftci, N.S., Int.J. Photoenergy, **5** (2003)199.
[5] I.Gur, N.A. Fromer, M.L. Geier, A.P. Alivisatos, Science**, 310** (2005) 462-465.
[6] X. Peng, Nano Res. **2** (2009) 425-447.
[7] I. Riedel, J.Riediger, J.Ohland, J.Keller, M. Knipper, J.Parisi, R.Mainz, and S.Merdes, Solar Energ. Mater. and Solar Cells*,* **95,** (2011) 270-273.
[8] F. Smaili, M. P. Brown and K. Austin, Appl. Phys. Letters **54,** (2011) 10304.
[9] N.A. Goryunova, The Chemistry of Diamond like Semiconductor, MIT, Cambridge, MA (1965) 142.
[10] F. Fray, P. Lloyd, Thin Solid Films **58**, (1979) 29.
[11] J. A. Lvarez-Garcia, J. Macros-Ruzafa, A. Perez-Rodrguez, A. Romano-Rodrıguez, J.R. Morante, R. Scheer, Thin Solid Films **361/362** (2000) 208.
[12] S. Peng, J. Liang, L. Zhang, Y. Shi, J. Chen, J. of Crys. Growth **305** (2007) 99–103.
[13] M. Krunks, O. Kijatkina, H. Rebane, I. Oja, V. Mikli, A. Mere, Thin Solid Films **403/404** (2002) 71.
[14] P. Bera, C.H. Kim and S.I. Seok. Polyhedron, **27** (2008) 3433.
[15] J.G. Dunna, C. Muzenda, Thermochim. Acta, **369** (2001) 117.
[16] K. Kondo, S. Nakamura, K. Sato, Jpn. J. Appl. Phys. **37** (1998) 5728.
[17] R. Hunger, M. Wilhelm, K. Diesner, Proceedings of the Second World Conference on Photovoltaic Solar Energy Conversion, Vienna, Austria, July (1998).
[18] K. Kambas, J. Spyridelis, M. Balkanski, Phys. Stat. Sol. B, **105** (1981) 29.
[19] Enzenhofer, T.Unold, T.Schock, Physica Status Solidi A, **203** (2006) 2624-2629.
[20] J. Qiu, Z. Jin, J. Qian, Y. Shi, W. Wu, J. of Crys. Growth, **282** (2005) 421–428.